# Mercury's capture into the 3/2 spin-orbit resonance as a result of its chaotic dynamics

**Alexandre C. M. Correia**[1,2] **& Jacques Laskar**[2]

[1]*Departamento de Física da Universidade de Aveiro, Campus Universitário de Santiago, 3810-193 Aveiro, Portugal*
[2]*Astronomie et Systèmes Dynamiques, IMCCE-CNRS UMR8028, Observatoire de Paris, 77 Avenue Denfert-Rochereau, 75014 Paris, France*

**Mercury is locked into a 3/2 spin-orbit resonance where it rotates three times on its axis for every two orbits around the sun[1–3]. The stability of this equilibrium state is well established[4–6], but our understanding of how this state initially arose remains unsatisfactory. Unless one uses an unrealistic tidal model with constant torques (which cannot account for the observed damping of the libration of the planet) the computed probability of capture into 3/2 resonance is very low (about 7 per cent)[5]. This led to the proposal that core–mantle friction may have increased the capture probability, but such a process requires very specific values of the core viscosity[7,8]. Here we show that the chaotic evolution of Mercury's orbit can drive its eccentricity beyond 0.325 during the planet's history, which very efficiently leads to its capture into the 3/2 resonance. In our numerical integrations of 1,000 orbits of Mercury over 4 Gyr, capture into the 3/2 spin-orbit resonant state was the most probable final outcome of the planet's evolution, occurring 55.4 per cent of the time.**

Tidal dissipation will drive the rotation rate of the planet towards a limit equilibrium value $x_1(e)n$ depending on the eccentricity $e$ and on the mean motion $n$ (see Methods). In a circular orbit ($e = 0$) this equilibrium coincides with synchronization ($x_1(0) = 1$), but $x_1(e_0) = 1.25685$ for the present value of Mercury's eccentricity ($e_0 = 0.206$), while the equilibrium rotation rate $3n/2$ is achieved for $e_{3/2} = 0.284927$. In their seminal work[5], Goldreich and Peale assumed that Mercury passed through the 3/2 resonance during its initial spin-down. They derived an analytical estimate of the capture probability into the 3/2 resonance and found $P_{3/2} = 6.7\%$ for the eccentricity $e_0$. With the updated value of the momentum of inertia[9] $(B - A)/C \simeq 1.2 \times 10^{-4}$, this probability increases to 7.73%, and our numerical simulations with the same setting give $P_{3/2} = 7.10\%$ with satisfactory agreement.

In fact, using the present value of the eccentricity of Mercury is questionable, as the eccentricity undergoes strong variations in time, owing to planetary secular perturbations. Assuming a random date for the crossing of the 3/2 resonance for 2,000 orbits, we found numerically $P_{3/2}^{\mathrm{BVW50}} = 3.92\%$ and $P_{3/2}^{\mathrm{BRE74}} = 5.48\%$ for these secular (averaged) solutions of Brouwer and Van Woerkom[10] and Bretagnon[11]. It should be stressed that with the regular quasiperiodic solutions BVW50 or BRE74, as for the fixed value of the eccentricity $e_0$, the 3/2 resonance can be crossed only once, because $e < e_{3/2}$. This will no longer be the case with a complete solution for Mercury's orbit that takes into account its chaotic evolution[12,13]. In this case, Mercury's eccentricity can exceed the characteristic value $e_{3/2}$ (Fig. 1), and additional capture into resonance can occur.

To check this new scenario, it is not possible to use a single orbital solution because, owing to its chaotic behaviour, the motion cannot be predicted precisely beyond a few tens of millions of years. We have thus performed a statistical study of the past evolutions of Mercury's orbit, with the integration of 1,000 orbits over 4 Gyr in the past, starting with very close initial conditions. This statistical study was made possible by the use of the averaged equations for the motion of the Solar System[12,13] that have recently been readjusted and compared to recent numerical integrations[14], with very good agreement over nearly 35 Myr.

Owing to the chaotic evolution, the density function of the 1,000 solutions over 4 Gyr is a smooth function (Fig. 1), similar, but not equal, to a gaussian curve[14]. The mean value of the eccentricity $\bar{e}_{\mathrm{LA04}}$ is slightly higher than $\bar{e}_{\mathrm{BVW50}}$ and $\bar{e}_{\mathrm{BRE74}}$, but the main difference is a much wider range for the eccentricity variations, from nearly zero to more than 0.45. The planet eccentricity can now increase beyond $e_{3/2}$ during its history. Even if these episodes do not last for a long time, they will allow additional capture into the 3/2 spin-orbit resonance.

For each of these 1,000 orbital motions of Mercury, we have numerically integrated the rotational motion of the planet, taking into account the resonant terms of equation (2), for $p = k/2$ with $k = 1,\ldots,10$, the tidal dissipation, and the planetary perturbations, starting at $t_0 = -4$ Gyr, with a rotation period of 20 days. Because $e$ is not constant, the ratio $x(t)$ of the rotation rate of the planet to its mean motion $n$ will tend towards a limit value $\tilde{x}_1(t)$ (see Methods) that is similar to an averaged value of $x_1(e(t))$, and capture into resonance can now occur in various ways.

Type I is the classical case, where $e < e_p$ (Fig. 2a). It is only in this case that the probability formula of Goldreich and Peale[5] will apply. In type II, the eccentricity oscillates around $e_p$ at the time when the spin rate $x(t)$ decreases towards $p$. The tidal dissipation thus drives $x(t)$ several times across $p$, greatly increasing the probability of capture (Fig. 2b). Types I and II can only occur in the first few Myr, as the spin rate decreases from faster rotations. We distinguish these cases from type III, where the planet is not initially captured into

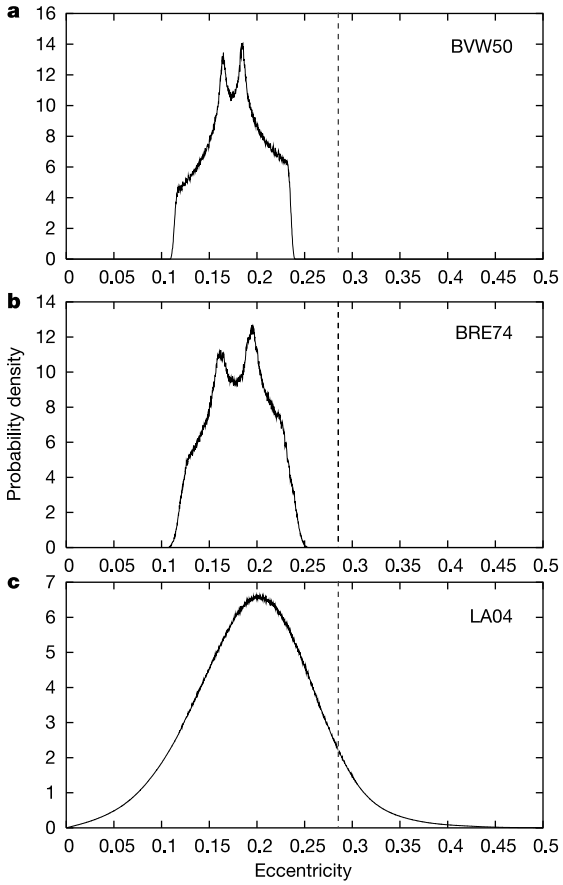


**Figure 1** Probability density function of Mercury's eccentricity. Values are computed over 4 Gyr for the two quasiperiodic solutions BVW50 (ref. 10) (**a**) and BRE74 (ref. 11) (**b**) and for the numerical integration of the secular equations of refs 12 and 14 for 1,000 close initial conditions (LA04, **c**). The mean values of the eccentricity in these solutions are respectively $\bar{e}_{\mathrm{BVW50}} = 0.177$, $\bar{e}_{\mathrm{BRE74}} = 0.181$, and $\bar{e}_{\mathrm{LA04}} = 0.198$. The vertical dotted line is the characteristic value $e_{3/2}$.

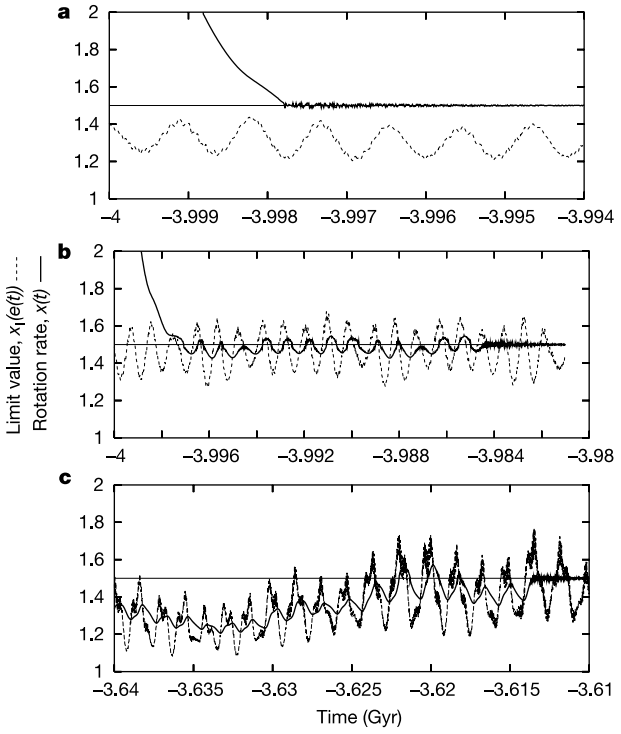


**Figure 2** Typical cases of capture into the 3/2 resonance. The rotation rate $x(t)$ (bold curve) and limit value $x_1(e(t))$ (dotted curve) are plotted versus time (Gyr). **a**, Type I is the classical case[5]: As $e < e_{3/2}$, the limit value $x_1$ is always lower than 3/2. **b**, In Type II, at the time when $x$ reaches the resonant value 3/2, $e$ is oscillating around $e_{3/2}$, leading to multiple crossings of the resonance, with ultimately a capture. **c**, Type III corresponds to solutions that have not been captured during the initial crossing of the resonance, but later on, as the eccentricity increases beyond $e_{3/2}$.

resonance $p$; but later on, as the orbital elements evolve, the eccentricity increases beyond $e_p$, and tidal dissipation accelerates the spin rate beyond $p$, leading to additional capture (Fig. 2c).

Over 1,000 orbits, a few were initially trapped in high-order resonances (one in 7/2, one in 4/1, two in 9/2 and three in 5/1), but these were associated with high values of the planet's eccentricity. As the eccentricity decreased these resonances became unstable, and none of these high-order resonances survived. They did eventually get trapped for a long time into the 5/2 resonance, but even that did not survive over the full history of the planet. Indeed, the stability of the resonances depends on the eccentricity of Mercury, and except for the 1/1 resonance, the resonances may become unstable for very small values of the eccentricity (Table 1).

We followed all 1,000 solutions, starting from −4 Gyr, until they reached the present date or were captured into the 2/1, 3/2 or 1/1 resonances. Unlike in previous studies, we found that capture into the 1/1 resonance is possible, because the eccentricity of Mercury may decrease to very low values at which capture can occur and the resonance remain stable. Over 554 solutions that were captured into the 3/2 resonance, a single one, initially captured at −3.995 Gyr, escaped from resonance at about −2.396 Gyr. The solution then got trapped into the 1/1 resonance at −2.290 Gyr, capture that was favoured by the very low eccentricity required to destabilize the 3/2 resonance (Table 1). Out of the 56 solutions initially trapped into the 2/1 resonance, ten were destabilized, and only two of them were further captured, one into the 3/2 resonance, and one into the 1/1 resonance. Globally, we obtained a final capture probability:

$$P_{1/1} = 2.2\%, \quad P_{3/2} = 55.4\%, \quad P_{2/1} = 3.6\% \tag{1}$$

The remaining 38.8% non-resonant solutions end with nearly the same final rotation rate of $x_f = 1.21315$, because all the orbital solutions are very close in the vicinity of the origin. Among the solutions captured into the 3/2 resonance, we can distinguish 31 solutions of type I, 168 of type II and 355 of type III (Fig. 2).

Table 1 **Critical eccentricity $e_c(p)$ for the resonance $p$**

| $p$ | $e_c(p)$ |
|---|---|
| 1/1 | – |
| 3/2 | 0.000026 |
| 2/1 | 0.004602 |
| 5/2 | 0.024877 |
| 3/1 | 0.057675 |
| 7/2 | 0.095959 |
| 4/1 | 0.135506 |
| 9/2 | 0.174269 |
| 5/1 | 0.211334 |

If $e < e_c(p)$, the resonance $p$ becomes unstable, and the solution may escape the resonance. The critical eccentricity $e_c(p)$ is obtained by the resolution of $[\Omega(e)p - N(e)]/H(p,e) = (3/2K)\, n[(B-A)/C]$.

With the consideration of the chaotic evolution of the eccentricity of Mercury, we thus show that with a realistic tidal dissipative model that properly accounts for the damping of the libration of the planet, and without the need for some additional core–mantle friction, the present 3/2 resonant state is the most probable outcome for the planet.

Additionally, from the present state of the planet, we can derive an interesting constraint on its past evolution. Of all 554 orbits trapped into the 3/2 resonance, for 521 of them (94.0%) Mercury's eccentricity exceeded 0.325 in the past 4 Gyr. The conditional probability that Mercury's eccentricity exceeded 0.325, given that its rotation is trapped into the 3/2 resonance, is thus 94.0%. The 3/2 resonant state of Mercury thus becomes an observational clue that the chaotic evolution of the planet orbit led its eccentricity beyond 0.325 over its history.

The largest unknown in this study remains the dissipation factor $k_2/Q$ of $K$ (equation (4)) (ref. 15). A stronger dissipation would increase the probability of capture into the 3/2 resonance, because $x(t)$ would follow more closely $x_1(e(t))$ (Fig. 2), whereas lower dissipation would slightly decrease the capture probability. This study should apply more generally to any extrasolar planet or satellite whose eccentricity is forced by planetary perturbations. □

## Methods

Tidal dissipation and core–mantle friction will drive Mercury's obliquity (the angle between the equator and the orbital plane) close to zero. For zero-degree obliquity, and in the absence of dissipation, the averaged equation for the rotational motion near resonance $p$ (where $p$ is a half-integer) is[4,5]:

$$\dot{x} = -\frac{3}{2} n \frac{B-A}{C} H(p,e)\ \sin 2(\ell - pM) \tag{2}$$

where $\ell$ is the rotational angle, $x = \dot{\ell}/n$ is the ratio of the rotation rate to the mean motion $n$, $M$ is the mean anomaly and $H(p, e)$ are Hansen coefficients[5,16]. The moments of inertia are $A < B < C$, with $C = \xi mR^2$, where $m$ and $R$ are the mass and radius of the planet, and $\xi$ is a structure constant.

Tidal models independent of the frequency (constant-$Q$ models) do not account for the damping of the amplitude of libration that is at present observed on Mercury[5,17]. Moreover, these models introduce discontinuities into the equations and can thus be considered as unrealistic approximations for slow rotating bodies[18]. Therefore, we use here for slow rotations a viscous tidal model, with a linear dependence on the tidal frequency. Its contribution to the rotation rate is given by[5,18,19,20]:

$$\dot{x} = -K[\Omega(e)x - N(e)] \tag{3}$$

with $\Omega(e) = (1 + 3e^2 + 3e^4/8)/(1-e^2)^{9/2}$, $N(e) = (1 + 15e^2/2 + 45e^4/8 + 5e^6/16)/(1-e^2)^6$, and

$$K = 3n \frac{k_2}{\xi Q} \left(\frac{R}{a}\right)^3 \left(\frac{m_0}{m}\right) \tag{4}$$

where $k_2$ and $Q$ are the second Love number and the quality factor, while $a$, $m$ and $m_0$ are the semi-major axis, the mass of the planet and the solar mass, respectively. Equilibrium is achieved when $\dot{x} = 0$, that is, for constant $e$, when $x = x_1(e) = N(e)/\Omega(e)$.

For a non-constant eccentricity $e(t)$, the limit solution of equation (3) is no longer $x_1(e)$, but more generally:

$$\tilde{x}_1(t) = \left(x(0) + K\int_0^t N(e(\tau))g(\tau)\mathrm{d}\tau\right)/g(t) \tag{5}$$

where $g(t) = \exp(K\int_0^t \Omega(e(\tau))\mathrm{d}\tau)$.

Using $\xi = 0.3333$, $k_2 = 0.4$ and $Q = 50$ (refs 15, 21), we have $K = 8.45324 \times 10^{-7}\,\mathrm{yr}^{-1}$. Assuming an initial rotation period of Mercury of 10 h, we estimated that the time needed to despin the planet to the slow rotations would be about 300 million years. This is why we started our integrations in the slow-rotation regime, with a rotation period of 20 days ($x \approx 4.4$) and a starting time of $-4$ Gyr, although these values are not critical.

Received 12 March; accepted 4 May 2004; doi:10.1038/nature02609.


1. Pettengill, G. H. & Dyce, R. B. A radar determination of the rotation of the planet Mercury. *Nature* **206,** 1240 (1965).
2. McGovern, W. E., Gross, S. H. & Rasool, S. I. Rotation period of the planet Mercury. *Nature* **208,** 375 (1965).
3. Colombo, G. Rotation period of the planet Mercury. *Nature* **208,** 575 (1965).
4. Colombo, G. & Shapiro, I. I. The rotation of the planet Mercury. *Astrophys. J.* **145,** 296–307 (1966).
5. Goldreich, P. & Peale, S. J. Spin orbit coupling in the Solar System. *Astron. J.* **71,** 425–438 (1966).
6. Counselman, C. C. & Shapiro, I. I. Spin-orbit resonance of Mercury. *Symp. Math.* **3,** 121–169 (1970).
7. Goldreich, P. & Peale, S. J. Spin-orbit coupling in the solar system 2. The resonant rotation of Venus. *Astron. J.* **72,** 662–668 (1967).
8. Peale, S. J. & Boss, A. P. A spin-orbit constraint on the viscosity of a Mercurian liquid core. *J. Geophys. Res.* **82,** 743–749 (1977).
9. Anderson, J. D., Colombo, G., Espsitio, P. B., Lau, E. L. & Trager, G. B. The mass, gravity field, and ephemeris of Mercury. *Icarus* **71,** 337–349 (1987).
10. Brouwer, D. & Van Woerkom, A. J. J. The secular variations of the orbital elements of the principal planets. *Astron. Pap. Am. Ephem.* **XIII,** part II, 81–107 (1950).
11. Bretagnon, P. Termes à longue périodes dans le système solaire. *Astron. Astrophys.* **30,** 141–154 (1974).
12. Laskar, J. The chaotic motion of the solar system. *Icarus* **88,** 266–291 (1990).
13. Laskar, J. Large-scale chaos in the Solar System. *Astron. Astrophys.* **287,** L9–L12 (1994).
14. Laskar, J. *et al.* Long term evolution and chaotic diffusion of the insolation quantities of Mars. *Icarus* (in the press).
15. Spohn, T., Sohl, F., Wieczerkowski, K. & Conzelmann, V. The interior structure of Mercury: what we know, what we expect from BepiColombo. *Planet. Space Sci.* **49,** 1561–1570 (2001).
16. Hansen, P. A. Entwickelung der products einer potenz des radius vectors mit dem sinus oder cosinus eines vielfachen der wahren anomalie in reihen. *Abhandl. K. S. Ges. Wissensch.* **IV,** 182–281 (1855).
17. Murray, C. D. & Dermott, S. F. *Solar System Dynamics* (Cambridge Univ. Press, Cambridge, 1999).
18. Correia, A. C. M. & Laskar, J. Néron de Surgy, O. Long term evolution of the spin of Venus. I. Theory. *Icarus* **163,** 1–23 (2003).
19. Munk, W. H. & MacDonald, G. J. F. *The Rotation of the Earth; A Geophysical Discussion* (Cambridge Univ. Press, Cambridge, 1960).
20. Kaula, W. Tidal dissipation by solid friction and the resulting orbital evolution. *J. Geophys. Res.* **2,** 661–685 (1964).
21. Yoder, C. F. Astrometric and geodetic properties of Earth and the Solar System. *Glob. Earth Physics: A Handbook of Physical Constants* 1–31 (American Geophysical Union, Washington DC, 1995).


**Acknowledgements** This work was supported by PNP-CNRS, Paris Observatory CS, and Fundação para a Ciência e a Technologia, POCTI/FNU, Portugal. The numerical computations were made at IDRIS-CNRS, and Paris Observatory. Authors are listed in alphabetic order.

**Competing interests statement** The authors declare that they have no competing financial interests.

**Correspondence** and requests for materials should be sent to J.L. (Laskar@imcce.fr).

# Laser-induced ultrafast spin reorientation in the antiferromagnet $TmFeO_3$

**A. V. Kimel[1], A. Kirilyuk[1], A. Tsvetkov[1], R. V. Pisarev[2] & Th. Rasing[1]**

[1]*NSRIM Institute, University of Nijmegen, Toernooiveld 1, 6525 ED Nijmegen, The Netherlands*
[2]*Ioffe Physico-Technical Institute, 194021 St.-Petersburg, Russia*

**All magnetically ordered materials can be divided into two primary classes: ferromagnets[1,2] and antiferromagnets[3]. Since ancient times, ferromagnetic materials have found vast application areas[4], from the compass to computer storage and more recently to magnetic random access memory and spintronics[5]. In contrast, antiferromagnetic (AFM) materials, though representing the overwhelming majority of magnetically ordered materials, for a long time were of academic interest only. The fundamental difference between the two types of magnetic materials manifests itself in their reaction to an external magnetic field—in an antiferromagnet, the exchange interaction leads to zero net magnetization. The related absence of a net angular momentum should result in orders of magnitude faster AFM spin dynamics[6,7]. Here we show that, using a short laser pulse, the spins of the antiferromagnet $TmFeO_3$ can indeed be manipulated on a timescale of a few picoseconds, in contrast to the hundreds of picoseconds in a ferromagnet[8–12]. Because the ultrafast dynamics of spins in antiferromagnets is a key issue for exchange-biased devices[13], this finding can expand the now limited set of applications for AFM materials.**

To deflect the magnetization of a ferromagnet from its equilibrium, a critical field $H_{\mathrm{cr}}^{\mathrm{FM}} \approx H_{\mathrm{A}}$ of the order of the effective anisotropy field is required. In contrast, the response of an antiferromagnet to an applied field remains very weak before the exchanged-enhanced critical field $H_{\mathrm{cr}}^{\mathrm{AFM}} \approx \sqrt{H_{\mathrm{A}} H_{\mathrm{ex}}}$ is reached. In most materials the exchange field $H_{\mathrm{ex}} \gg H_{\mathrm{A}}$ ($H_{\mathrm{A}} < 1\,\mathrm{T}$, $H_{\mathrm{ex}} \approx 100\,\mathrm{T}$) and thus $H_{\mathrm{cr}}^{\mathrm{AFM}} \gg H_{\mathrm{cr}}^{\mathrm{FM}}$. This difference is related to the fact that in an antiferromagnet, no angular momentum is associated with the AFM moment. This large rigidity of an antiferromagnet to an external field also shows up in the magnetic resonance frequency[14], where spin excitations start at $\omega \approx \gamma\sqrt{H_{\mathrm{A}} H_{\mathrm{ex}}}$. This is in contrast to $\omega \approx \gamma H_{\mathrm{A}}$ in a ferromagnet, which can result in a difference of more than two orders of magnitude.

Indeed, dynamical many-body theory calculations[15] show a possibility of AFM dynamics with a time constant of a few femtoseconds only. Experimentally, the ultrafast dynamics of an antiferromagnet is still an intriguing question. The problem however is far from trivial, as there is no straightforward method for the manipulation and detection of spins in AFM materials. Therefore, an appropriate mechanism should be found that would deflect the AFM moments on a timescale down to femtoseconds, and this change should subsequently be detected on the same timescale.

The solution to this problem can be found in the magnetocrystalline anisotropy. Indeed, a rapid change of this anisotropy can lead, via the spin–lattice interaction, to a reorientation of the spins[11,12]. Such anisotropy change, in turn, can be induced by a short femtosecond laser pulse in a material with a strong temperature-dependent anisotropy. The subsequent reorientation of the spins can be detected with the help of time-resolved linear magnetic birefringence[16], which enables us to follow the change of the direction of spins in antiferromagnets, similar to the Faraday and Kerr effects in ferromagnets.

The rare-earth orthoferrites $RFeO_3$ (where R indicates a rare-earth element) investigated here are known for a strong temperature-dependent anisotropy[17,18]. These materials crystallize in an orthorhombically distorted perovskite structure, with a space-group symmetry $D_{2h}^{16}$ (*Pbnm*). The iron moments order antiferromagnetically, as shown in Fig. 1, but with a small canting of the spins on different sublattices. The temperature-dependent anisotropy energy has the form[19,20]:

$$\Phi(T) = \Phi_0 + K_2(T)\sin^2\theta + K_4\sin^4\theta \qquad (1)$$

where $\theta$ is the angle in the $x$–$z$ plane between the $x$ axis and the AFM moment **G**, see Fig. 1, and $K_2$ and $K_4$ are the anisotropy constants of second and fourth order, respectively. Applying equilibrium conditions to equation (1) yields three temperature regions corresponding to different spin orientations:

$$\Gamma_4(G_{\mathrm{x}}\ F_{\mathrm{z}}):\ \theta = 0,\ T \geq T_2$$

$$\Gamma_2(G_{\mathrm{z}}\ F_{\mathrm{x}}):\ \theta = 1/2\pi,\ T \leq T_1$$

$$\Gamma_{24}:\ \sin^2\theta = K_2(T)/2K_4,\ T_1 \leq T \leq T_2 \qquad (2)$$

where $T_1$ and $T_2$ are determined by the conditions $\mathrm{K}_2(T_1) = -2K_4$